



Research article

Understanding the Dynamics of Polymer Extrusion: Simulation of Thermoplastics Processing with Planetary Roller Extruders

Mario Radwan^{a,*}, Steffen Schneider^{b,1}, Thomas Ernst Müller^b, Sulamith Frerich^a^a Ruhr-Universität Bochum, Virtualization of Process Technology, Universitätsstr. 150, 44801 Bochum, Germany^b Ruhr-Universität Bochum, Carbon Sources and Conversion, Universitätsstr. 150, 44801 Bochum, Germany

ARTICLE INFO

Keywords:

Polymer processing
Polymer extrusion
Planetary roller extruder
Numerical modelling
CFD simulation
Validation
Fluid dynamics
Material stress

ABSTRACT

Resource efficient processing of polymers is of paramount importance to minimize energy consumption, processing time, and material losses in the polymer industry. This study is concerned with polymer processing in planetary roller extruders. A three-dimensional numerical flow simulation was tailored to understand the polymer flow through the extruder in detail. Using the simulation software ANSYS Polyflow, we quantified both directly measurable process parameters, such as pressure build-up, and more intangible parameters, such as material shear. By varying operational and material parameters in a sensitivity analysis, we showed that the dynamics, material stress and pressure build-up are controlled primarily by the number of spindles and their rotational speed. Notably, this work provides the first successful validation of a 3D simulation of a polymer flow in a planetary roller extruder against actual experimental data. The simulation showed robust agreement between the simulated and experimental values, provided that a critical backpressure length is reached. This computational approach minimizes labor-intensive experimental testing in polymer processing.

1. Introduction

Polymers play a pivotal role in various industries, serving as a cornerstone material with increasing production volumes. According to PlasticsEurope [1], 390.7 million tons of polymers were processed into manifold products in 2021, a substantial increase from the 365.5 million tons produced in 2018. This is related to advantages, such as lightweight and cost-effective production of polymers, compared to alternative materials. However, polymers are not without their drawbacks. Conventionally, they are carbon-based and primarily derived from fossil raw materials, mostly petroleum [2–4]. To mitigate the environmental impact, it is urgent to reduce the carbon footprint of polymer products. This can be done by replacing fossil raw materials with recycled or bio-based polymers [5] or by increasing the resource efficiency in the processing of the polymer. Given their often short lifespan the disposal of these products poses significant environmental challenges due to their poor biodegradability [2].

Extrusion is an important processing method for polymers with a share of approximately two-thirds of the production volume [6]. Extruders are categorized according to their internal design as single-screw and multi-screw extruders [7,8]. The latter includes, i.e., the planetary roller extruder (PRE). The design of PREs resembles a planetary gear (see Fig. 1). The main spindle (MSP) drives meshing

* Corresponding author.

E-mail addresses: radwan@vvp.rub.de (M. Radwan), schneider@ls-csc.rub.de (S. Schneider), mueller@ls-csc.rub.de (T.E. Müller), frerich@vvp.rub.de (S. Frerich).

¹ contributed equally.

Abbreviations

CAD	Computer aided design
CFD	Computational fluid dynamics
MSP	Main spindle
MST	Mesh superposition technique
PA6	Polyamide 6
PE-HD	High-density polyethylene
PE-LLD	Linear low-density polyethylene
PRE	Planetary roller extruder
PS	Polystyrene
PSP	Planetary spindle
RC	Roller cylinder
SSE	Single screw extruder
TSE	Twin screw extruder

Symbols

a_T	[–] Temperature shift factor
A_0	[Pa s] Zero shear viscosity
A^*	[–] Auxiliary variable for the calculation of the back pressure length
B	[s] Reciprocal transition shear rate
b_{Channel}	[m] Channel width
b_{Mesh}	[m] Mesh width
B^*	[–] Auxiliary variable for the calculation of the back pressure length
C	[–] Slope of the viscosity curve in the pseudoplastic viscosity range
C^*	[–] Auxiliary variable for the calculation of the back pressure length
$\Delta p/\Delta z$	[Pa m ⁻¹] Pressure gradient
E_0	[J mol ⁻¹] Activation energy
f	[N m ⁻³] Volume related forces
h_{Channel}	[m] Channel height
h_{Mesh}	[m] Mesh height
K	[Pa s ⁿ] Consistency factor
$L_{\text{Backpressure}}$	[m] Back pressure length
m	[kg m ⁻³ K ⁻¹] Temperature-related increase in density
n	[–] Power law index
n_{MSP}	[s ⁻¹] Main spindle speed
n_{rel}	[s ⁻¹] Relative speed between main and planetary spindle in experiment (exp) or simulation (sim)
$n_{\text{R,PSP}}$	[s ⁻¹] Rotational spindle speed
N_T	[–] Number of teeth
$N_{T,\text{Rest}}$	[–] Number of remaining teeth
p	[Pa] Pressure
$p_{\text{Measurement}}$	[Pa] Measured pressure
R	[J mol ⁻¹ K ⁻¹] Universal gas constant
T	[K] Temperature
T_0	[K] Reference temperature
v	[m s ⁻¹] Local velocity vector
v_{MSP}	[m s ⁻¹] Velocity of the main spindle
v_z	[m s ⁻¹] Velocity in axial direction
$\dot{\gamma}$	[s ⁻¹] Shear rate
η	[Pa s] Shear viscosity
$\pi\dot{V}$	[–] Dimensionless volume flow
ρ	[kg m ⁻³] Density
ρ_0	[kg m ⁻³] Density at temperature of 0 °C

planetary spindles (PSP) that rotate inside a stationary internally toothed roller cylinder (RC). The 45° helical gearing provides axial material transport with simultaneous radial cross-mixing. Advantages of PREs over other extruder designs include modular design, precise temperature control, and low shear rates [8].

Process development on the PRE is complex due to the large number of possible settings, including spindle configuration, rotational speed of the main spindle, and the mass flow. For this reason, extensive experimental studies are carried out to improve process

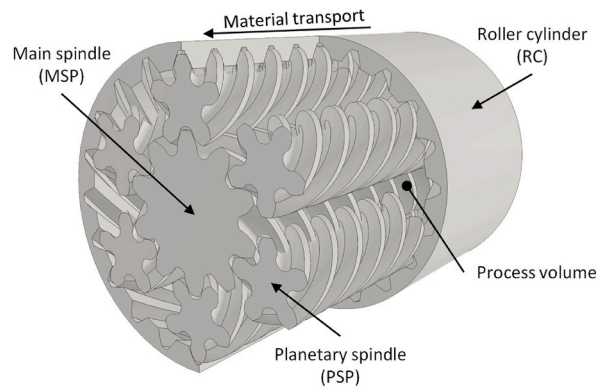


Fig. 1. Internal design of a PRE with main spindle (MSP), planetary spindles (PSP), and roller cylinder (RC).

efficiency and product quality. Due to the relatively high material mass flows required and the associated energy consumption for drive and heating, these trials are resource intensive. Because the PRE consists of a non-transparent roller cylinder that defines the processing volume, researchers are prevented from making qualitative assessments or visual observations during processing. In addition, temperature, pressure and shear rates in the polymer melt are difficult to measure. To improve process development, we decided to complement the experimental investigations with simulations. Our target was to nurture the understanding of the polymer dynamics in PREs and thereby help to decrease the number of required experiments. This is linked to a reduction in the carbon footprint during process development and production.

Over the past few years, numerous experimental and numerical studies were carried out on the effects of operating parameters on extruding operations. For single- and twin-screw extruders, there is already a large number of investigations and models available to describe and optimize the processes, respectively [9–13]. Previous experimental work on PREs has focused on their compounding behavior [14–16] and the scale-up process [17], among other things. Mathematical PRE models, such as those developed by Rudloff et al., are based on experimental data and calculate process variables such as the degree of melting or the residence time along the cylinder of a PRE [18,19].

However, three-dimensional CFD (computational fluid dynamics) simulations, which can provide detailed information on the processes occurring in the PRE, are rare due to the system's high complexity. Birr has developed a simplified model to investigate the processing of long-fiber-reinforced thermoplastics [20]. The simulated flow profiles are of qualitative nature. A deeper insight into a PRE through numerical simulation of the flow field and mixing dynamics was gained by Winck and Frerich. However, the results and the simulative setup could not be validated [21]. Based on the latest developments in experimental research on PRE [22], experimental data can now be used to validate simulative results.

The primary objective of this publication is to further extend the understanding of the fluid dynamics inside a PRE. This study aims to enable a faster process development with a reduced number of necessary experiments, leading to a higher product quality and a more efficient and, thus, environmentally friendly production process. To achieve this goal, a three-dimensional computer aided design (CAD) model of a PRE was created, which was then used for CFD simulations. To ensure the accuracy of the results, the CFD simulation of the planetary roller extruder was validated for the first time using real measurement data from literature. Process parameters, such as spindle configuration, main spindle speed, and mass flow were varied. These investigations focus on analyzing the main influencing factors of the pressure build-up characteristics and the mechanical shear stress on the material. With this knowledge, processes can be specifically optimized and adjusted with regard to product quality and process efficiency.

2. Methodology

2.1. Simulation methods

The CFD simulations were set up using the commercial software ANSYS Polyflow 2020 R1. According to the conditions of the extrusion process and the properties of the polymer, the following assumptions were made: (1) The fluid is incompressible. (2) The flow is laminar. (3) The sticking condition between walls and fluid is valid. (4) Gravitational forces are neglected. (5) The polymer flow is considered a generalized Newtonian flow; viscoelastic effects are neglected. (6) The simulated roller cylinder section is completely filled with polymer at all times. Thus, single-phase flow exists. (7) Changes in temperature are negligible. Thus, an isothermal calculation is performed.

With these assumptions, the Navier-Stokes equations simplify to the following conservation equations (Eq. 1 and Eq. (2)) for mass and momentum [23,24],

$$\nabla \cdot v = 0$$

Eq. 1

$$\rho \cdot \left(\frac{\partial v}{\partial t} + (v \cdot \nabla)v \right) = f - \nabla p + \eta \cdot \Delta v \quad \text{Eq. 2}$$

where v is the local velocity vector, ρ is the density, f is for volume related forces, p is the pressure, and η stands for shear viscosity. Other extruder simulations also use these simplified assumptions [25,26]. We have challenged these assumptions in non-isothermal calculations and by varying the inlet pressure and did not see significant effects on the calculated results.

To validate the results of the simulation, the calculated values were compared with experimental data. Rudloff et al. performed experiments using a custom-built cylinder to measure the melt pressure axially along the extrusion direction [22]. The simulation was set up to use the experimentally measured melt pressure for validation. This validated methodology was the basis for our investigations into the operating characteristics of the PRE.

2.2. Geometry of the planetary roller extruder and mesh for computation

The PRE can vary in the number of modules. Within a module there are sections with different degrees of filling [20]. The downstream section of each module is more filled, so the assumption of complete filling is more likely to apply. Studies by Rudloff show that process conditions such as pressure build-up and material stress are particularly influential in this section [18]. Based on this and in order to avoid excessive computation time, only the fully filled section of a PRE module was modelled. The results calculated for this section can be applied to other filled regions of the PRE. The PRE section was modelled by using the Autodesk Inventor Professional 2020 CAD software. The model included the main spindle, the roller cylinder, and a variable number of planetary spindles and was constructed based on published geometry data [8,27–29]. The length of the simulated section corresponded to the pitch length of the planetary spindle of 55.536 mm.

For the computation, equations (1) and (2) were solved in a discretized computational domain. There are several approaches for discretizing computational domains with moving components [30,31]. Since the process volume, in which the polymer flow changes with each movement of the extruder, constant remeshing would be required. To avoid this time-consuming remeshing, the Mesh Superposition Technique (MST) was applied [24]. In this technique, the moving components of the PRE (Fig. 2a) and the fluid domain (Fig. 2b) are meshed separately and then superimposed. At each computational step, a check is made to see if a fluid element is superimposed on a solid body. The actual process volume results from the fluid elements that are not overlapped.

The zone of fluid domain elements that intermesh with machine components is of particular interest for analysis because of the high shear rates that occur in these finite volumes. Therefore, all intermeshing sections were meshed at a higher resolution than the melt channels, which contain only fluid domain elements (Fig. 2). Since there are no direct interactions between the machine components, a coarser mesh is sufficient. Zones covered by moving components during a complete rotation do not need to be meshed.

The kinematics of the PRE were adapted to further reduce the computational complexity of the simulation. In the actual setup, the roller cylinder is stationary as the outer machine housing, while the planetary spindles rotate around the main spindle (Fig. 3a). To reduce the mesh size and, thus, the computational complexity, the kinematics of the system were adapted so that each component had only one degree of freedom. Thus, the roller cylinder was rotated in the simulation while the planetary spindles were fixed in place, and the fine and coarse mesh regions were fixed in a stationary position. This approach has already been reported elsewhere [21,27].

Fig. 3 shows the PRE kinematics in the actual experiment (Fig. 3a) compared to the simulation (Fig. 3b). The orange arrows represent the direction of the rotation of these spindles, which is the same in experiment and simulation. However, the motion of the gear (blue arrow) was transferred from the planetary spindles (a) to the roller cylinder (b). This requires adjusting the relative rotational speed (n_{rel} , Eq. (3)) of the main spindle (n_{MSP}) and the planetary spindles ($n_{R,PSp}$) [18]:

$$n_{rel} = n_{MSP} - n_{R,PSp} \quad \text{Eq. 3}$$

In the real system design, the rotational speed of the planetary spindles around the main spindle due to the gearing is (Eq. (4)):

$$n_{R,PSp,Exp} = 1/3 \cdot n_{MSP} \quad \text{Eq. 4}$$

The combination of Eq. (3) and Eq. (4) results in a relative velocity that is expressed by Eq. (5):

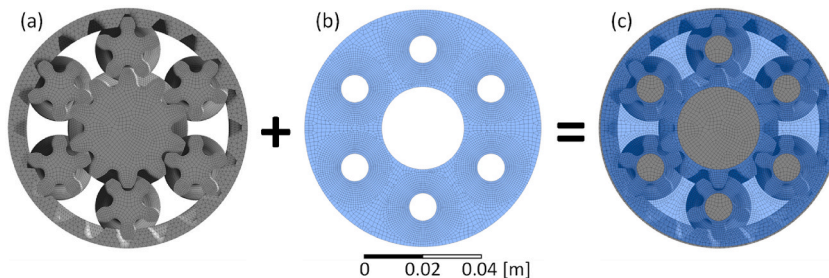


Fig. 2. Computational meshes of (a) the machine components of the PRE, (b) the fluid domain, and (c) superimposition of the meshes. The inner circular zone is permanently overlaid by solids and therefore did not need to be meshed.

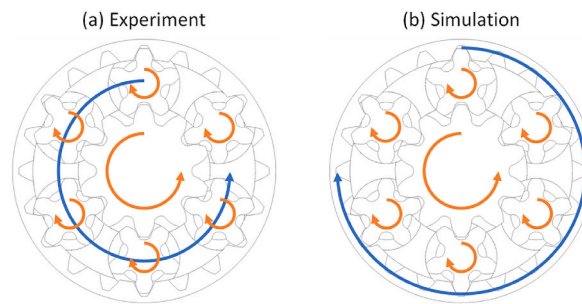


Fig. 3. PRE kinematics. The orbiting motion of the planetary spindles from the experiment (a) is transferred into a rotation of the roller cylinder for the simulation (b).

$$n_{rel,Exp} = 2/3 \bullet n_{MSP} \quad \text{Eq. 5}$$

As mentioned above, the planetary spindles are stationary in the simulation and rotate only around their own axis. The rotary movement of the planetary spindles around the main spindle is therefore eliminated. This results in Eq. (6) for calculating the relative speed in the simulation:

$$n_{rel,Sim} = n_{MSP} \quad \text{Eq. 6}$$

A comparison of Eq. (5) and Eq. (6) shows that the relative speeds of the main and planetary spindles change when the PRE kinematics are adjusted. Since this could distort the simulation results, the speed of each PRE component is multiplied by a factor of 2/3 in the simulation, respectively. As a result, the relative velocities correspond to those of the experiments (see also [27]). For the sake of simplicity, the speeds in this paper always refer to the main spindle speed of the experiment.

2.3. Scope of the simulation

The parameters specified were spindle configuration (number) and speed of the main spindle, material and temperature (which determine the viscosity and density of the melt) and mass flow. For validation purposes, a total of 25 experimental operating points with different parameters were modelled in the simulation. The corresponding operating parameters of the comparative experiment can be found in Ref. [22].

The simulations for our sensitivity analysis (see Table 1) included all available degrees of freedom to provide insights into the system that would be difficult or impossible to measure experimentally. It was designed by first defining a default operating point with the following settings: The material being processed is PE-HD with a spindle configuration of six standard spindles. The mass flow was 40 kg h^{-1} at a spindle speed of 120 min^{-1} . The temperature is set at $200 \text{ }^\circ\text{C}$. To investigate the parameter's influence on the extrusion process, only one of the input variables was changed in a respective analysis (see italic table entries). Then, the simulation results were compared with the standard operating point, allowing the effects to be analyzed individually, without any other influencing variables.

2.4. Polymer data

The simulation included polymers with different molecular structures. The materials were chosen to be the same as for experiments reported in the literature, namely polyamide 6 ("PA6" – Ultramid B3S from BASF SE), high-density polyethylene ("PE-HD" – Vestolen A6060 from Sabic), linear low-density polyethylene ("PE-LLD" – Lufflexen 18 TFA from LyndellBasell), and polystyrene ("PS" – 143 E from BASF SE). For numerically solving the system of equations, the material data models included the temperature and shear rate dependent viscosity (Table 2 and Fig. 4) and the temperature dependent melt density (Eq. (10) and Table 2).

The Carreau model (Eq. (7)) and the power approach (Eq. (8)) were used to describe the viscosity, analogous to the work of Rudloff [18]. The temperature dependence of the viscosity of the polymer melt was described by the Arrhenius temperature shift factor (Eq.

Table 1
Parameter field covered during the simulation.

Polymer	Number of spindles [-]	Mass flow [kg h^{-1}]	Spindle speed [min^{-1}]	Temperature [$^\circ\text{C}$]
<i>PE-HD</i>	6	40	120	<i>170, 185, 200, 215, 230</i>
<i>PE-LLD</i>	6	40	120	<i>170, 185, 200, 215, 230</i>
<i>PS</i>	6	40	120	<i>170, 185, 200, 215, 230</i>
<i>PA6</i>	6	40	120	<i>170, 185, 200, 215, 230</i>
PE-HD	3, 4, 5, 6	40	120	200
PE-HD	6	<i>20, 30, 40, 50, 60</i>	120	200
PE-HD	6	40	<i>40, 80, 120, 160, 200</i>	200

The variable that has been subject to variation is shown in italics.

Table 2

Data for calculating the viscosity and density of the materials [18,22].

	PA6	PE-HD	PE-LLD	PS
A_0 [Pa s]	218	12,582	1751	7800
B [s]	0.002	0.100	0.010	0.300
C [-]	0.54	0.87	0.77	0.70
E_0 [J mol ⁻¹]	60,049	6338	27,970	73,716
T_0 [°C]	260	200	200	200
K [Pa s ⁿ]	13,507.40	92,913.92	58,707.22	18,108.21
n [-]	0.46	0.13	0.23	0.30
ρ_0 [kg m ⁻³]	1035	858	821	1070
m [kg m ⁻³ °C ⁻¹]	0	0.462	0.423	0.513

(9)). At the start of each simulation, the viscosity coefficients were calculated for the temperature of interest and implemented in the simulation as a shear rate-dependent function. This fitted the material data to the desired temperature and allowed the simulations to be run isothermally. As an example, the shear rate-dependent viscosity at 200 °C is shown in Fig. 4.

$$\eta(\dot{\gamma}, T) = \frac{a_T(T) \bullet A_0}{(1 + a_T(T) \bullet B \bullet \dot{\gamma})^C} \quad \text{Eq. 7}$$

$$\eta(\dot{\gamma}, T) = K \bullet a_T^n(T) \bullet \dot{\gamma}^{n-1} \quad \text{Eq. 8}$$

$$a_T(T) = \exp\left(\frac{E_0}{R} \left(\frac{1}{T} - \frac{1}{T_0}\right)\right) \quad \text{Eq. 9}$$

The melt density was calculated as a linear model with the parameters ρ_0 (density at a temperature of 0 °C) and m (slope of the straight line as a function of temperature in °C) according to the method of Rudloff [22]. The values are valid for the single phase melting range. The density was then calculated for the temperature of interest according to Eq. (10):

$$\rho(T) = \rho_0 + m \bullet T \quad \text{Eq. 10}$$

2.5. Mesh independence and validation methodology

The simulations were run on a Dell OptiPlex 7070 tower with an Intel CPU (Core i7-9700 with 8 cores) and 32 GB RAM. Depending on the material properties and the mesh size, the simulation took an average of 1:37 h. Especially, when the viscosity of the polymer deviated strongly from Newtonian behavior, the simulation took considerably longer.

To evaluate the influence of the variables under investigation, the extensive simulation data need to be converted into interpretable results. Thus, the simulation data has to be carefully selected to include only the relevant regions in the evaluation. Thus, neither data within inlet and outlet areas were considered. By excluding these regions, distorted results were avoided. Only the data from the fluid domain within the PRE was balanced, since this region describes the fluid region that is relevant for the evaluation of, e.g., the material stress. It was also taken into account that the values may be differing at each cross-section, e.g., in the melt channel or the intermeshing area. To make a representative statement, volume-related mean values were calculated either for each cross-section plane along the extruder or for the total volume, depending on the representative evaluation. Arithmetic averaging was not used here, because some more densely meshed regions (see section 2.2) would falsify the results. The simulation data's output was produced directly from the used simulation software ANSYS. Self-written MATLAB scripts were used for further analysis.

One aim of this work is to develop a validated simulation of the extrusion process in a PRE. In this work, the results of the simulation were mainly validated in three ways. First, the independence of the simulation results from the computational mesh used was investigated. Second, the results of the mesh-independent simulation were compared with experimental measurement data from literature to determine the values' correctness. Third, as the final step, error considerations analyzed possible deviations that may occur despite the preceding validation steps.

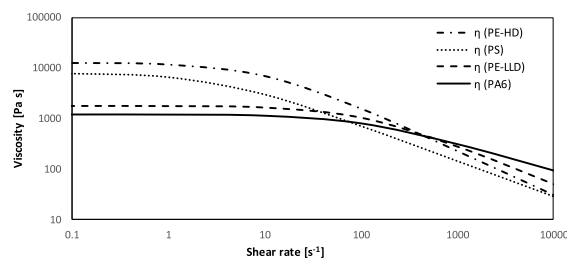


Fig. 4. Viscosity of chosen polymers as a function of shear rate at 200 °C, based on viscosity data from Refs. [18,22].

Constructing a mesh with elements of high quality and appropriate size is critical to obtain meaningful simulation results. A mesh convergence study ensured that the applied mesh had no significant effect on the results. Consequently, the PRE geometry and fluid domain under study were systematically meshed with elements of varying sizes. The element size ranged from 1.00 mm to 2.50 mm with a step size of 0.25 mm. Regions that require finer meshing were assigned a factor and therefore received smaller element sizes. The goal of the mesh convergence analysis was to determine the optimum element size for maximum accuracy and minimum simulation time. For this purpose, a monitor variable had to be determined and the influence of the element size on this variable was observed. As for the validation studies, the pressure difference between the inlet and outlet of the extruder was used as monitored variable.

For a PRE configuration with six planetary spindles, Fig. 5 shows that the pressure difference approaches a limit value as the number of elements increases in each case. However, simultaneously increasing the number of elements and reducing their size does not result in any further improvement in accuracy. In contrast, the simulation time increases as the number of elements increases. Thus, the mesh with a global element size of 1.50 mm was selected. This element size satisfies both the requirements of accuracy and simulation time efficiency. Fig. 5 shows that a further reduction of element size leads to no significant improvement; accordingly, the independence of simulation results from the mesh can be considered as given. Since identical behavior was observed for other spindle configurations as well, the global element size of 1.50 mm was set.

In addition, to ensure reliability of the simulation in process development, it is necessary to verify the correctness of the results. Since the simulation covers only a section and not the entire PRE, the simulated results have to be compared with experimental measurements. However, conventional roller cylinders only show limited options for measuring parameters in-line. Rudloff has conducted experimental investigations to analyze the process conditions inside the roller cylinder [18,22]. He thus fabricated and used a unique roller cylinder, with measurement opportunities spaced 45 mm apart along its length. This particular cylinder makes it easier to compare simulation and experimental data. Rudloff [22] measured the pressure and temperature values at three locations inside the roller cylinder. Since his 45 mm measuring distance between two sensor positions is less than the 55.536 mm in this work's simulated PRE, it was ensured that the PRE simulation covers a length that is encompassed by two sensors.

To investigate the input variables' relative influences, the calculations were applied to different materials, operating points, and spindle configurations. By varying the test parameters and recording the aforementioned sensor values in the roller cylinder, the measured data allow a validation of the simulation. Sanjabi et al. have previously applied a similar validation approach based on pressure and temperature values for a single screw extruder [32,33].

In this work, the PRE simulation assumes a completely filled roller cylinder. As Birr's work [20] has shown, the percentage of filling increases towards the end of the roller cylinder, where the assumption of a complete filling is most justified. Thus, the downstream sensors were selected for validation. Using Rudloff's mathematical model for the back pressure length [18,22], it was possible to verify the percentage of filling in the simulated roller cylinder section as follows.

The PRE generates pressure in the conveying direction against the constriction components (e.g., nozzle), due to the helical gearing of the planetary spindles. The resulting pressure gradient ($\Delta p/\Delta z$) is affected by factors such as spindle configuration, rotational speed, and mass flow. The pressure gradient ($\Delta p/\Delta z$) and the measured pressure ($p_{Measurement}$) were used to calculate the length of material backed up in front of the downstream cross-sectional constriction of the roller cylinder ($L_{Backpressure}$), as per to Eq. (11).

$$L_{Backpressure} = \frac{p_{Measurement}}{\Delta p/\Delta z} \tag{Eq. 11}$$

Eq. (12) was used to calculate the pressure gradient ($\Delta p/\Delta z$) required for the back pressure length. The model assumes plug flow, which is represented by a stepped filling degree curve. In reality, the curve continues to rise continuously.

$$\Delta p / \Delta z = \frac{\pi \dot{V} - A^*}{B^* \cdot C^*} \tag{Eq. 12}$$

The dimensionless volume flow $\pi \dot{V}$ and the auxiliary variables A^* , B^* , and C^* were calculated according to Eq. (13) to Eq. (16):

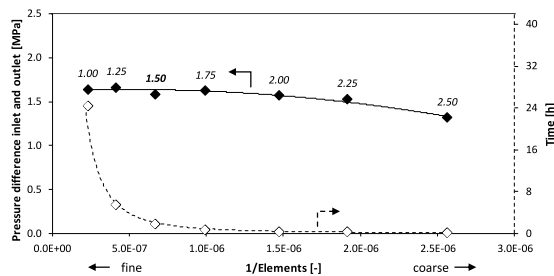


Fig. 5. Pressure difference between inlet and outlet of the simulated section and calculation time as a function of inverse element count. The data labels show the global element size in millimeters. The lines provide an optical guide for the eye.

$$\pi_{\dot{V}} = \frac{\dot{V}}{N_{PSP} \bullet 0.5 \bullet h_{mesh} \bullet b_{mesh} \bullet v_z \bullet \frac{N_{T,Rest}}{N_T}} \quad \text{Eq. 13}$$

$$A^* = 1 - \frac{h_{mesh}^{n+1} \bullet v_{MSP}^n \bullet N_{T,Rest}}{h_{channel}^{n+1} \bullet v_z^n \bullet N_T} \quad \text{Eq. 14}$$

$$B^* = 1 + \frac{h_{channel}^{n+2} \bullet v_Z^{n-1} \bullet b_{channel} \bullet N_{T,Rest}}{h_{mesh}^{n+2} \bullet v_{MSP}^{n-1} \bullet b_{mesh} \bullet N_T} \quad \text{Eq. 15}$$

$$C^* = \frac{h_{mesh}^{n+1}}{6 \bullet K \bullet v_Z^n \bullet \frac{N_{T,Rest}}{N_T}} \quad \text{Eq. 16}$$

The number of planetary spindles N_{PSP} , and the geometric quantities h_{mesh} , b_{mesh} , $h_{channel}$, and $b_{channel}$ mentioned in the above equations were derived from the PRE's gearing data. The parameters v_{MSP} and v_Z are functions of the geometry and the main spindle speed. The consistency factor K and the flow exponent n are parameters that describe the viscosity of the melt. The number of teeth on the selected spindles, and the simulated spindle configuration in general, is accounted for by the use of N_T and $N_{T,Rest}$. The volume flow rate of the polymer melt is represented by \dot{V} . In this study, the measured pressure ($p_{Measurement}$) was the value of the downstream pressure sensor, since it indicates the maximum pressure value in the considered cross-section. The pressure gradient can be used to calculate the back pressure length opposite the flow direction. Since the back pressure length varies proportionally with the degree of filling, it is a good measure to evaluate the simulation's accuracy.

3. Results and discussion

The CFD simulation was designed to study the operating characteristics of a PRE in detail. For this purpose, a 3D model of a PRE section was constructed and a fluid, in this case a homogeneous polymer melt, was computed to flow through it. The simulation was validated with reported experimental data from 25 experiments performed by Rudloff [22]. The process characteristics were investigated in terms of the axial pressure build-up and the stress on the material in form of the shear rate. The operating parameters of number of spindles, spindle speed, mass flow, and the polymer type were varied to gain a comprehensive understanding of the system. The results for the PRE show what make it different from other extruder designs.

3.1. Validation of the simulation results

To evaluate the simulation's quality, the difference between the pressure values of simulation and experiment was calculated and divided by the value of experimental pressure near the nozzle. Fig. 6 shows a plot of this ratio against the calculated back pressure length. The ratio describes the absolute deviation between simulation and experiment according to the actual pressure level, and the graph illustrates how the simulation quality depends on the back pressure length.

When the back pressure length is equal to or greater than 55 mm, the deviation between the simulation and experiment is small and lies within a tolerance band of $\pm 20\%$ normalized to the pressure level (Fig. 6). Within this range, a complete filling of the extruder is assumed, and the simulation results can be considered as valid. However, the deviation between simulation and experiment increases for small back pressure lengths. Two effects seem likely for the increasing deviation between simulation and experiment. One is that the pressure level is generally lower when the back pressure length is smaller. Thus, a ratio of both yields a higher level. However, a second effect to be considered is that the simulation assumes complete filling and maximum pressure build-up. In reality, the pressure build-up is not fully developed, which also contributes to a large deviation.

As previously stated, simulations as models of reality involve several simplifications. In this work, simulation accuracy depends on pressure level and pressure gradients. In addition, the pressure level influences the accuracy of the measured values. The measured

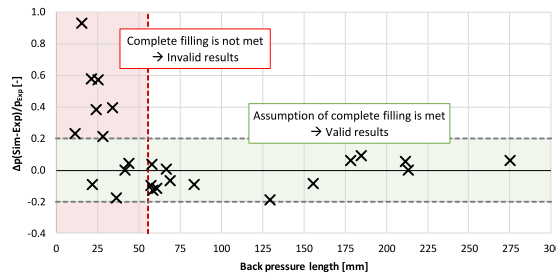


Fig. 6. Difference between the pressure calculated in the simulation and the experimentally determined pressure as a function of the back pressure length, the distance the material accumulates before the downstream cross-sectional constriction. From a back pressure length of 55 mm, the assumption of a completely filled roll cylinder is considered to be satisfied.

published data are reported with an accuracy of ± 0.025 MPa. Simulations provide results with finer resolution. They can cause a significant relative error due to sensor inaccuracy, particularly at low-pressure levels.

It is also important to note that the simulations were performed isothermally. As a result, they took into account neither the development of shear heat nor heat entry into the polymer from the two heated components, the main spindle and roller cylinder. This approach can also be found elsewhere [27]. The negligible temperature increase in the short simulation section involved does not compromise accuracy, as evidenced by measured data from Rudloff's experimental studies [22]. To minimize the error arising from the neglected temperature, the melt viscosity is raised to the set temperature level by temperature shift, resulting in values that approximate the expected ones.

Thus, based on the validation considerations, the following simulation considers completely filled roller cylinders to be reliable and sufficiently accurate.

3.2. Material stress in the extrusion process

Polymers experience different types of stress during extrusion on PRE. The influencing factors can be grouped as external stresses (including temperature, oxygen concentration, and mechanical stress) and internal stresses (including chemical composition and physical structure) [34]. In order to achieve the highest possible product quality, the different types of stresses should be kept to a minimum.

Due to the structure of the simulations performed, not all of the aforementioned aging factors could be investigated. Since the simulations are isothermal, a description of the thermal stress is not part of this work. The same applies to the strain on the chemical and physical structure, since the interactions between the different substances would have to be considered. However, the simulations yield the shear rate. As an indicator of the mechanical stress in the polymer melt, the shear rate can cause the polymer chains to break. This section examines how the various process input variables and the material selection affect the shear rate and, thus, the polymer melt. With this knowledge, the process can be designed for the lowest possible shear rates, which supports the achievement of high-quality products.

The PRE includes rotating (main spindle, planetary spindles) and static (roller cylinder) components. As described above, the process volume was divided into two areas, intermeshing sections and melt channels. Both types of areas are surrounded by two planetary spindles, the roller cylinder, and the main spindle. With regard to the different areas mentioned within the PRE cross section, the point at which the shear rate is examined is vital.

Fig. 7 contains contour plots showing the shear rate within PRE cross sections. The figure's left part shows a longitudinal section along the PRE. Its plane section is indicated by red lines on the PRE cross section on the right. The maximum and average shear rates depend to a relevant extent on the melt temperature, the material's viscosity, and the rotational speed. Therefore, the first step is a qualitative analysis of the shear rate distribution.

The cross-section shows that the lowest shear rates are present within the melt channels. The minimum shear rate drops independently of the operating settings to 0 s^{-1} . Accordingly, the polymer chains experience little or no mechanical stress inside the melt channels. The opposite is the case in the intermeshing sections, where the highest shear rates are present. Slightly elevated shear rates are also present on the non-engaged tooth flanks. In the longitudinal section, it is noticeable that the relationships described above do not change along the PRE's length. Irrespective of the axial position, the highest shear rates are observed directly on the tooth flanks and especially in the intermeshing regions. These results qualitatively agree with Winck's simulations and Rudloff's calculations [18,

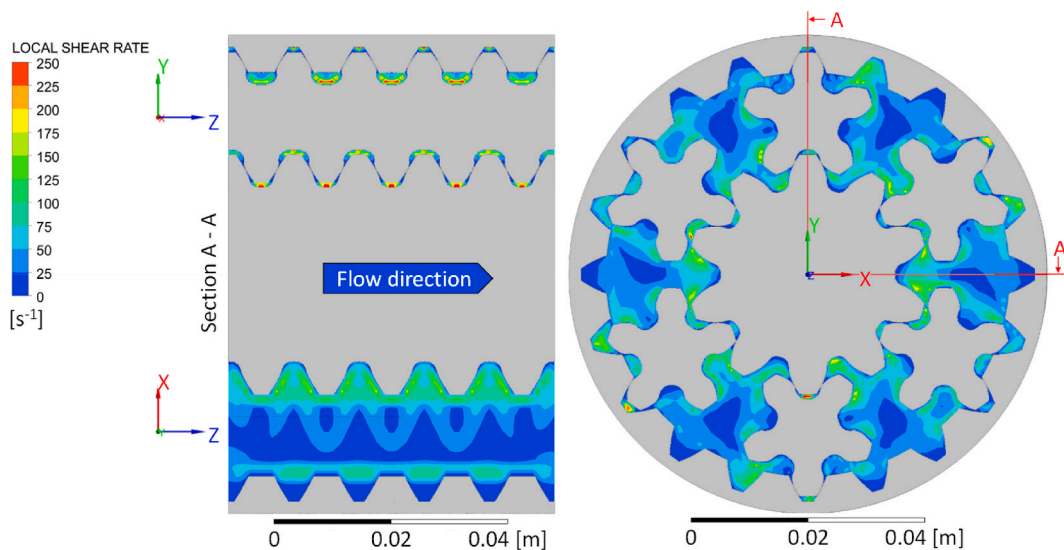


Fig. 7. Computed shear rates in the cutting planes along the XY-, YZ-, and XZ-directions.

21].

To analyze the shear rates, a volume-averaged representative shear rate was calculated based on the total process volume depending on the operating condition. Fig. 8 plots the described parameters at standard operating conditions (6 PSP, 40 kg h⁻¹, 120 min⁻¹, see simulation plan above) for different materials at different temperatures.

It is illustrated that the material has little effect on the level of the mean shear rate. At a simulated temperature of 200 °C, the values vary in an interval from 85.8 s⁻¹ to 93.7 s⁻¹. The differences in the mean shear rate can be explained by the melt's viscosity. As the viscosity decreases, the molecules become more agile and the polymer chains can be deformed more easily. Correspondingly, the shear increases with decreasing viscosity as the internal shear resistance of the material decreases. PA6 has the lowest zero viscosity (218 Pa s), followed in ascending order by PE-LLD (1751 Pa s), PS (7800 Pa s), and PE-HD (12,582 Pa s). The average mean shear rates of the materials, evaluated at a melt temperature of 200 °C, are in the inverted order (PA6 93.7 s⁻¹, PE-LLD 91.5 s⁻¹, PS 88.8 s⁻¹ and PE-HD 85.8 s⁻¹).

However, it is noticeable that the mean shear rate for PA6, for example, increases with increasing temperature, even though the PE-HD value remains more or less the same across temperatures. This effect is attributed to the temperature dependence of the two materials' melt viscosity. Assuming a shear rate of 90 s⁻¹, which is approximately the average mean shear rate, the viscosity level of PA6 decreases by a factor of 4.07 when heated from 170 °C (1656 Pa s) to 230 °C (407 Pa s). The corresponding value of the PE-HD viscosity level drop from 170 °C (1737 Pa s) to 230 °C (1661 Pa s) is 1.05. Thus, PA6's viscosity is considerably more temperature-dependent than is the case for PE-HD. The same applies to the shear rates. At higher temperatures, the PA6's viscosity decreases, and, as a result, the shear rate increases. In the case of PE-HD, keeping the viscosity more or less constant means that the shear rate does not change either.

In addition to the choice of material and temperature setting discussed earlier, other PRE parameters are relevant to setting the process conditions. These include main spindle speed, mass flow, and spindle configuration. Fig. 9 illustrates the influence of each of these parameters on the mean shear rate. Simulations were performed for PE-HD at a temperature of 200 °C using the standard operating settings.

It can be seen that the spindle speed and the number of spindles have the highest influence on the mean shear rate and are thus most responsible for the material's shear. The shear rate at the minimum spindle speed of 40 min⁻¹ is 28.4 s⁻¹, while it increases to 143.3 s⁻¹ at the maximum spindle speed of 200 min⁻¹. Additional comparative studies on Single-Screw Extruders (SSE) and Twin-Screw Extruders (TSE) in addition to the presented PRE simulation have shown that an increase in rotational speed leads to a linear increase in the shear rate for all three extruder types studied [18,26,35–37]. Beyond this, the shear rate of the PRE increases with the number of planetary spindles from 42.8 s⁻¹ (three spindles) to 85.8 s⁻¹ (six spindles). These results concur with those of other simulative studies on PRE [18,21,22,27]. Winck's publications also include the type of planetary spindles as an additional degree of freedom, which has an increasing but overall small effect on the PRE's shear rate. By contrast, the mass flow through the PRE does not considerably affect the mean shear rate. The minimum mass flow of 20 kg h⁻¹ leads to a shear rate of 86.4 s⁻¹, while the maximum (60 kg h⁻¹) produces a rate of 85.2 s⁻¹. Here, the investigated parameter is constant over the simulated mass flow range. This result is consistent with Rudloff's models for shear rate in the PRE [18,22]. The shear rate in TSE is independent of the mass flow as well. In contrast, the mass flow influences the shear rates in SSE because of the dependency of rotational speed and mass flow.

In addition to the influencing variables described above, the gap height, i.e., the distance between two intermeshing system components, is relevant for the shear rate in the PRE. A study by Rudloff [22] showed that the shear rate decreases with increasing gap height. Due to the stationary fixation of the system components in the simulations performed, this influencing factor cannot be considered. A floating bearing of the planetary spindles corresponding to reality cannot be implemented at this point. However, the influence on the mean shear rate was assumed to be small, since the gap height decreases on one side, while increasing on the other. Since both effects cancel each other out and reduce the influence on the mean value, this factor was neglected here.

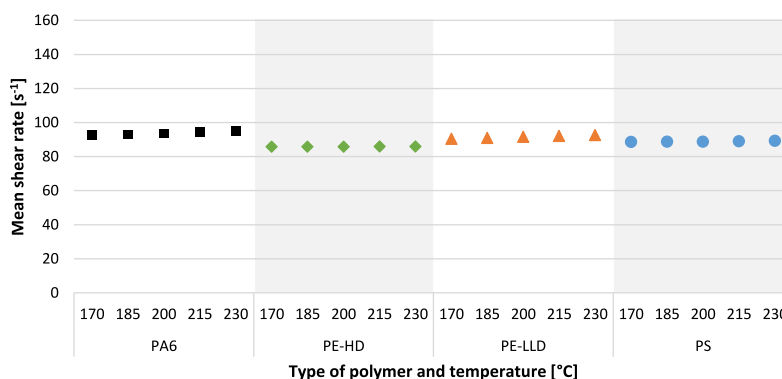


Fig. 8. Mean shear rates in the simulation section as a function of the type of the polymer and temperature at standard operating conditions (6 PSP, 40 kg h⁻¹, 120 min⁻¹).

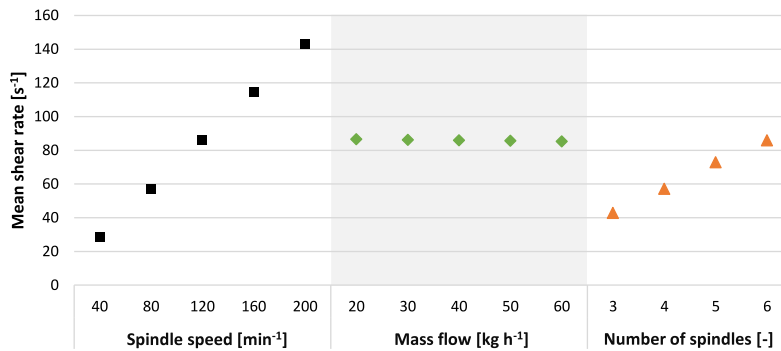


Fig. 9. Mean shear rate as a function of the operating parameters for the polymer PE-HD at 200 °C.

3.3. Pressure build-up characteristics

Due to the specific design of the PRE's geometry, the polymer melt accumulates at the end of the roller cylinder module, in front of flow resistances, such as dispersion rings or the die. These components, thus, give rise to built-up of back pressure during extrusion. For the polymer melt to pass the flow resistances, pressure is generated in the filled section of the roller cylinder by the motion of the helical-toothed components. Depending on the mass balance of in- and outflowing polymer, flow resistance and resulting pressure gradient, the roller cylinder is filled to a certain level. In this study, we investigated the pressure gradient as a function of operating parameters and to calculate the otherwise non-measurable parameters filling level and back pressure length. The knowledge gained allows the conveying efficiency of the PRE to be optimized by adjusting the system configuration and operating parameters.

Fig. 10 shows the pressures calculated for the inside of the PRE as a contour plot. The pressure distribution is analyzed qualitatively first. The pressure in the melt channel is relatively constant, while large changes in pressure occur around the spindles. The pressure depends on the position of the respective volume element in the intermeshing section. Within finite volumes where the tooth flanks of both the planetary spindles and the roller cylinder, or the planetary spindle and the main spindle engage (red ellipse), the available volume is reduced, causing the pressure in the melt to increase. In comparison, the pressure in finite volumes of diverging tooth flanks (blue ellipse) decreases, and can be even below the pressure of the melt in the channel. Note that the inlet pressure does not affect the pressure gradient.

In addition, we have investigated whether this is also the case for other polymers and at different operating parameters. Fig. 11 depicts the pressure gradient at standard operating conditions (6 PSP, 40 kg h⁻¹, 120 min⁻¹) for four different polymers as function of temperature.

In contrast to the mean shear rate, the pressure gradient shows a clear dependence on the choice of polymer and temperature. This

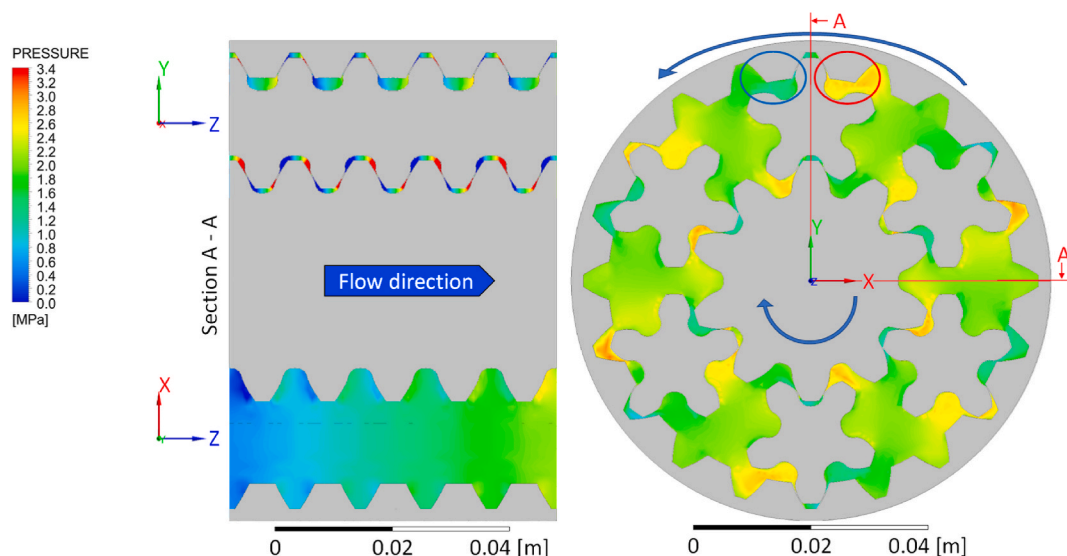


Fig. 10. Positioning of the planes for visualization and pressure distribution calculated for the XY-, YZ-, and XZ-planes. The regions of higher pressures where the teeth engage with one another can clearly be seen (red ellipse). In the region of diverging teeth, the pressure is reduced (blue ellipse). (For interpretation of the references to colour in this figure legend, the reader is referred to the Web version of this article.)

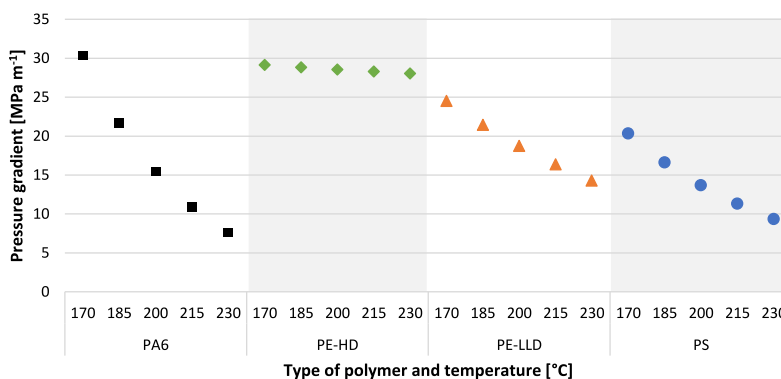


Fig. 11. Effects of the type of polymer and the choice of temperature on the pressure gradient at standard operating conditions (6 PSP, 40 kg h⁻¹, 120 min⁻¹).

effect is attributed to the material-specific viscosity and the associated temperature shift factor. At the standard operating temperature of 200 °C, PE-HD shows the highest pressure gradient (28.8 MPa m⁻¹). Slightly smaller pressure gradients are present if PE-LLD (18.8 MPa m⁻¹), PA6 (15.5 MPa m⁻¹), and PS (13.8 MPa m⁻¹) are used. The viscosity of the polymers follows the same sequence. While the viscosity of PE-HD at the considered temperature of 200 °C and the mean shear rate at 120 min⁻¹ is calculated to 1780 Pa s, the viscosity of PE-LLD is lower by a factor of 1.63 (1091 Pa s). PA6 (848 Pa s) and PS (788 Pa s) show even lower viscosities and, thus, lower pressure gradients.

This suggests that the pressure gradient is directly related to the viscosity of the polymer melt. The temperature dependence of the pressure gradient can be derived from the polymer specific temperature shift factor. In the temperature range from 170 °C to 230 °C, PA6 shows the strongest temperature dependence ($\Delta aT/\Delta T = -0.2237 \text{ K}^{-1}$). By contrast, PE-HD has the lowest temperature dependence, at -0.0035 K^{-1} . PS (-0.0538 K^{-1}) and PE-LLD (-0.0161 K^{-1}) rank in between. Consequently, both the choice of material and the set operating temperature strongly influence the pressure level and pressure gradient in the fully filled zone of the roller cylinder.

Fig. 12 illustrates the dependence of the pressure gradient on rotational speed, mass flow, and number of spindles. Although mass flow indicates a proportional relationship to the pressure gradient, rotational speed and number of spindles exhibit a nonlinear behavior. While an increase in rotational speed starting from 40 min⁻¹ (13.4 MPa m⁻¹) shows a large increase in the pressure gradient, it produces a lower change in the pressure gradient from 160 min⁻¹ (31.6 MPa m⁻¹) to 200 min⁻¹ (33.8 MPa m⁻¹). This relationship can be explained by the previously described increase in the mean shear rate and the associated change in viscosity. As seen above, the mean shear rate also increases with increasing rotational speed. Due to the structurally viscous behavior of the polymer melt, the viscosity is reduced according to the Carreau model. That means that the pressure build-up in the extruder is no longer as high and the pressure gradient decreases. The overall increase in the pressure gradient as a result of an increased rotational speed can be observed with SSE and TSE as well, as a comparison with other studies has shown [10,36,38,39].

If the mass flow is increased in the PRE, there is a linear decrease in the respective pressure gradient from 31.0 MPa m⁻¹ to 26.0 MPa m⁻¹. Due to the increased mass flow, the extruder's back pressure length, and thereby the pressure build-up zone, rises. This causes a long pressure build-up and, thus, a reduced pressure gradient. Previous experimental and simulative studies on SSE and TSE have observed a comparable behavior [12,40–42]. Upon varying the number of spindles, the effect of increased back pressure length is also relevant. However, if more planetary spindles are installed, the free volume within the roller cylinder is reduced. Thus, the back pressure length increases, resulting in a smaller pressure gradient as described above. However, additional planetary spindles add axial material transport, which itself increases the pressure gradient. Since this effect predominates, the pressure gradient also increases with a higher number of planetary spindles (from 7.4 MPa m⁻¹ to 28.6 MPa m⁻¹).

The simulative investigations on the pressure gradient show that the selection of the material and the processing temperature as well as the rotational speed and number of spindles have the greatest influence on the pressure build-up. A specific adjustment of the listed parameters will adapt the pressure level and directly influence the connected processing methods, such as injection molding.

4. Conclusions

To increase the sustainability of process development, digitization of experiments can help to reduce material and energy consumption. In the context of polymer processing, we developed for this purpose a validated three-dimensional CFD simulation to describe the dynamics of completely melted polymers in planetary roller extruders (PRE). To validate the three-dimensional model of a PRE section, the simulation results were compared with experimentally measured data. In a sensitivity analysis, system configuration, rotational speed, and mass flow were varied to study the effect of these parameters on pressure build-up and shear stress in the extruder. Adjustments to the simulation methodology are required to additionally simulate the melting process or entire PREs.

The pressure in the polymer melt is determined mainly by the flow resistance resulting from dispersion rings and the die geometry. The intermeshing zone of the tooth flanks of two converging PRE components results in an increased local pressure, while the local

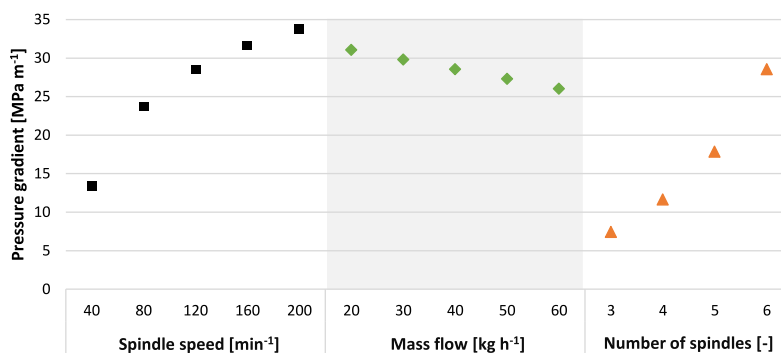


Fig. 12. Effects of the choice of operating parameters on the pressure gradient for the polymer PE-HD at 200 °C.

pressure decreases in the zones, where the tooth flanks diverge.

There is a steady increase in the pressure in the axial conveying direction of the PRE. This axial pressure gradient is independent of the absolute pressure. The pressure gradient, i.e. the pressure increase per extruder length, was computed to verify the filling level and to study the conveying efficiency of the PRE. Note that the assumption of a completely filled extruder is only fulfilled, when a critical back pressure length is exceeded. Under this condition, the agreement between simulation and experiment was within less than ± 20 %. If the modules are only partially filled, deviations in the simulation results may occur. Changes in mass flow have little effect on the pressure gradient. Critical parameters that lead to an increasing pressure gradient within the PRE are an increase in the number of spindles, rotational speed, and material viscosity.

Further, the shear rate in the PRE was investigated as a measure of the mechanical stress on the polymer. The experimentally validated simulations showed that the shear rates in the PRE vary significantly with the location of the finite volume. While low stress was found in the melt channels between two planetary spindles, high shear rates were found in the intermeshing zones. Therefore, the extruder design in the intermeshing sections should be developed further to reduce the mechanical stress on the polymer and ensure a good product quality.

Representative shear rates, corresponding to the volume-averaged value over the entire extruder flow region, were calculated to compare simulations performed for different settings. The representative shear rates increased sharply with the number of spindles and increasing rotational speed, while the material type and the mass flow rate had little effect. Therefore, when processing shear-sensitive polymers, the system should be designed with as few spindles as possible and high speeds should be avoided.

The methodology established in this study makes the development of extrusion processes more resource efficient. With the knowledge of the characteristic fluid dynamics, the geometry of the PRE and the processing can be optimally adapted to the specific polymer type and the subsequent processing steps. This reduces the number of the necessary experiments required during process development. The application of the simulation results within the context of scaling processes to different plant sizes helps to reduce material consumption, and has the potential to save significant costs. Deep insight into the fluid dynamics within the planetary roller extruder also helps to identify regions of high material stress to ensure the damage limits of the processed polymer materials are not exceeded. Furthermore, information how to improve the mixing performance and operating conditions for subsequent downstream processes can be drawn.

Ethics approval and consent to participate

Not applicable.

Data availability

Data will be made available on request.

CRediT authorship contribution statement

Mario Radwan: Writing – original draft, Visualization, Validation, Methodology, Formal analysis, Data curation, Conceptualization. **Steffen Schneider:** Writing – original draft, Software, Methodology, Investigation, Formal analysis, Data curation, Conceptualization. **Thomas Ernst Müller:** Writing – review & editing, Supervision, Project administration, Funding acquisition, Conceptualization. **Sulamith Frerich:** Writing – review & editing, Supervision, Project administration, Funding acquisition, Conceptualization.

Declaration of competing interest

The authors declare that they have no known competing financial interests or personal relationships that could have appeared to influence the work reported in this paper.

Acknowledgments

The research group Virtualization of Process Technology (VVP) thanks ENTEX Rust & Mitschke GmbH for the highly productive cooperation. This research was made possible by funding from the State of North Rhine-Westphalia, grant number IRR-2018-1, RWE Power AG, and the Faculty of Mechanical Engineering of Ruhr-Universität Bochum, as part of the endowed chair Carbon Sources and Conversion (CSC). St. S. is grateful for funding by CSC.

References

- [1] PlasticsEurope AISBL, *Plastics - the Facts 2022*, 2022. Brussels.
- [2] J. Hopewell, R. Dvorak, E. Kosior, Plastics recycling: challenges and opportunities, *Phil. Trans. R. Soc. B* 364 (1526) (2009) 2115–2126, <https://doi.org/10.1098/rstb.2008.0311>.
- [3] M. Bonnet, *Kunststofftechnik*, third ed., Springer Vieweg, Wiesbaden, 2016.
- [4] E. Baur, G. Harsch, M. Moneke, *Werkstoff-Führer Kunststoffe: Eigenschaften – Prüfungen – Kennwerte*, eleventh ed., Hanser, Munich, 2019.
- [5] P. Tomkins, T.E. Müller, Evaluating the carbon inventory, carbon fluxes and carbon cycles for a long-term sustainable world, *Green Chem.* 21 (15) (2019) 3994–4013, <https://doi.org/10.1039/c9gc00528e>.
- [6] M. Bonnet, *Kunststoffe in der Ingenieur Anwendung. STUDIUM*, Vieweg + Teubner, Wiesbaden, 2009.
- [7] H. Greif, A. Limper, G. Fattmann, *Technologie der Extrusion*, second ed., Hanser, Munich, 2017.
- [8] K. Kohlgrüber, M. Bierdel, H. Rust (Eds.), *Polymer-Aufbereitung und Kunststoff-Compoundierung: Grundlagen, Apparate, Maschinen, Anwendungstechnik*, Hanser, Munich, 2019.
- [9] A.L. Kelly, E.C. Brown, P.D. Coates, The effect of screw geometry on melt temperature profile in single screw extrusion, *Polym. Eng. Sci.* 46 (12) (2006) 1706–1714, <https://doi.org/10.1002/pen.20657>.
- [10] J. Covas, P. Costa, A miniature extrusion line for small scale processing studies, *Polym. Test.* 23 (7) (2004) 763–773, <https://doi.org/10.1016/j.polymertesting.2004.04.005>.
- [11] R.V. Chiruvella, Y. Jaluria, V. Sernas, M. Essegheir, Extrusion of non-Newtonian fluids in a single-screw extruder with pressure back flow, *Polym. Eng. Sci.* 36 (3) (1996) 358–367, <https://doi.org/10.1002/pen.10422>.
- [12] A. Eitzlmayr, G. Koscher, G. Reynolds, Z. Huang, J. Booth, P. Shering, J. Khinast, Mechanistic modeling of modular co-rotating twin-screw extruders, *Int. J. Pharm.* 474 (1–2) (2014) 157–176, <https://doi.org/10.1016/j.ijpharm.2014.08.005>.
- [13] B. Vergnes, Average shear rates in the screw elements of a corotating twin-screw extruder, *Polymers* 13 (2) (2021), <https://doi.org/10.3390/polym13020304>.
- [14] A. Limper, S. Seibel, C.-J. Wefelmeier, M. Roth, Homogeneous compounds, *Kunststoffe* 92 (11) (2002) 83–86.
- [15] A. Limper, S. Seibel, G. Fattmann, Compounding unit planetary roller extruder, *Macromol. Mater. Eng.* 287 (11) (2002) 815–823, <https://doi.org/10.1002/mame.200290011>.
- [16] T. Taufertshöfer, *Einfluss der Verfahrenstechnik eines Planetwalzenextruders auf die elektrische Leitfähigkeit rußgefüllter Polyolefine* (Ph.D. Thesis), University publisher of TU Berlin, Berlin, 2014.
- [17] M. Radwan, S.C. Frerich, Experimental study on the scalability of planetary roller extruders, *Chem. Eng. & Technol* (2023), <https://doi.org/10.1002/ceat.202200523>.
- [18] J. Rudloff, *Modellbildung und Vorabschätzung für das Betriebsverhalten eines Planetwalzenextruders*, 2021 (Ph.D. Thesis). Ilmenau.
- [19] J. Rudloff, M. Lang, K. Kretschmer, P. Heidemeyer, M. Bastian, M. Koch, A mathematical model describing the solid conveying and melting behavior of planetary roller extruders, in: *AIP Conference Proceedings*, 2014, pp. 592–595.
- [20] T. Birr, *Verarbeitung von langglasfaserverstärkten Thermoplasten für Spritzgussanwendungen auf dem Planetwalzenextruder*, 2016 (Ph.D. Thesis). Berlin.
- [21] J. Winck, S. Frerich, Numerical simulation of fluid flow and mixing dynamics inside planetary roller extruders, *Int. Polym. Proc.* 36 (5) (2021) 508–518, <https://doi.org/10.1515/ipp-2020-4084>.
- [22] J. Rudloff, K. Dietl, J. Kettemann, M. Lang, T. Hochrein, M. Bastian, C. Bonten, Schmelzesimulation des Planetwalzenextrusions-Prozesses. *Bildung & Forschung, Shaker, Düren*, 2021.
- [23] H. Oertel, *Prandtl – Führer durch die Strömungslehre*, Springer Fachmedien Wiesbaden, Wiesbaden, 2017.
- [24] ANSYS, Inc, *ANSYS Polyflow User's Guide*, 2021. Canonsburg, PA.
- [25] H. Tang, Y. Zong, L. Zhao, Numerical simulation of micromixing effect on the reactive flow in a co-rotating twin screw extruder, *Chin. J. Chem. Eng.* 24 (9) (2016) 1135–1146, <https://doi.org/10.1016/j.cjche.2016.04.040>.
- [26] D. Sun, X. Zhu, M. Gao, 3D Numerical simulation of reactive extrusion processes for preparing PP/TiO₂ nanocomposites in a corotating twin screw extruder, *Materials* 12 (4) (2019), <https://doi.org/10.3390/ma12040671>.
- [27] J.R. Winck, *Simulation und Visualisierung der Strömung und Durchmischung im Planetwalzenextruder für die Schaumextrusion von Polymilchsäure*, 2020 (Ph. D. Thesis). Bochum.
- [28] ENTEX Rust & Mitschke GmbH, *Verfahrenstechnisches Handbuch für den ENTEX Planetwalzenextruder L-WE30*, 2020. Bochum.
- [29] ENTEX Rust & Mitschke GmbH, *Entgasungstechnik mit dem ENTEX-Planetwalzenextruder*, 2020. Bochum.
- [30] R. Giguère, F. Bertrand, P.A. Tanguy, A three-dimensional mesh refinement strategy for the simulation of fluid flow with a fictitious domain method, *Comput. Chem. Eng.* 30 (3) (2006) 453–466, <https://doi.org/10.1016/j.compchemeng.2005.10.008>.
- [31] F. Bertrand, F. Thibault, L. Delamare, P.A. Tanguy, Adaptive finite element simulations of fluid flow in twin-screw extruders, *Comput. Chem. Eng.* 27 (4) (2003) 491–500, [https://doi.org/10.1016/S0098-1354\(02\)00236-3](https://doi.org/10.1016/S0098-1354(02)00236-3).
- [32] F. Sanjabi, S.R. Upreti, A. Lohi, F. Ein-Mozaffari, Helical flow of polymer melts in extruders, Part I: model development, *Adv. Polym. Technol.* 29 (4) (2010) 249–260, <https://doi.org/10.1002/adv.20195>.
- [33] F. Sanjabi, S.R. Upreti, A. Lohi, F. Ein-Mozaffari, Helical flow of polymer melts in extruders, Part II: model simulation and validation, *Adv. Polym. Technol.* 29 (4) (2010) 261–279, <https://doi.org/10.1002/adv.20193>.
- [34] G.W. Ehrenstein, S. Pongratz, *Beständigkeit von Kunststoffen*, Edition Kunststoffe, Hanser, Munich, 2007.
- [35] C. Rauwendaal, Scale-up of single screw extruders, *Polym. Eng. Sci.* 27 (14) (1987) 1059–1068.
- [36] K. Kohlgrüber (Ed.), *Hanser eLibrary. Der Gleichläufige Doppelschneckenextruder*, second ed., Hanser, Munich, 2016.
- [37] Z. Ke, H. Zhongqi, Y. Shupan, C. Wanghua, Numerical simulation for exploring the effect of viscosity on single-screw extrusion process of propellant, *Procedia Eng.* 84 (2014) 933–939, <https://doi.org/10.1016/j.proeng.2014.10.518>.
- [38] K. Wilczyński, A. Lewandowski, K.J. Wilczyński, Experimental study for starve-fed single screw extrusion of thermoplastics, *Polym. Eng. Sci.* 52 (6) (2012) 1258–1270, <https://doi.org/10.1002/pen.23076>.
- [39] P. Gorczyca, *Analyse und Optimierung von Einschnckenextrudern mit schnell drehenden Schnecken* (Ph.D. Thesis), Essen, 2011.

- [40] A. Lewandowski, K. Wilczyński, Modeling of twin screw extrusion of polymeric materials, *Polymers* 14 (2) (2022), <https://doi.org/10.3390/polym14020274>.
- [41] T. Fukuoka, Numerical analysis of a reactive extrusion process. Part II: simulations and verifications for the twin screw extrusion, *Polym. Eng. Sci.* 40 (12) (2000) 2524–2538, <https://doi.org/10.1002/pen.11383>.
- [42] A. Limper (Ed.), *Verfahrenstechnik der Thermoplastextrusion*, Hanser, Munich, 2012.